Konrad-Zuse-Zentrum für Informationstechnik Berlin
Heilbronner Str. 10, D-1000 Berlin 31

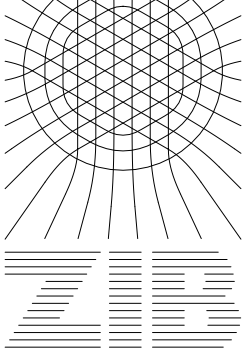

Jochen Fröhlich, Kai Schneider

Computation of Decaying Turbulence in an Adaptive Wavelet Basis

Preprint SC 96-11 (October 1996)

Computation of Decaying Turbulence in an Adaptive Wavelet Basis

Jochen Fröhlich [1] , Kai Schneider [2]

Abstract

The paper presents computations of decaying two–dimensional turbulence in an adaptive wavelet basis. At each time step the vorticity is represented by an adaptively selected set of wavelet functions which adjusts to the instantaneous distribution of vorticity. The results of this new algorithm are compared to a classical Fourier method and a Fourier method supplemented with wavelet compression in each time step.

Contents

[1]Konrad–Zuse–Zentrum Berlin, Heilbronner Str. 10, D-10711 Berlin-Wilmersdorf. Present address: Institut für Hydromechanik, Universität Karlsruhe, Kaiserstraße 12, D-76128 Karlsruhe

[2]Institut für Chemische Technik, Universität Karlsruhe, Kaiserstraße 12, D-76128 Karlsruhe

1 Introduction

Two–dimensional turbulent flows have been the subject of many theoretical and experimental investigations. Apart from their relevance for meteorology, flows in shallow rivers, and other applications they also serve as a test belt for the different concepts developed to understand the dynamics of turbulence. Although the precise mechanisms in the two–dimensional case are somewhat different from the three–dimensional case, main ideas may nevertheless be transfered.

A convenient means of investigation for two–dimensional flows is their direct numerical simulation. When focussing on the intrinsic mechanisms of turbulence, homogeneous, isotropic conditions are generally considered with the influence of boundaries being removed by imposing periodicity of the solution in both coordinate directions.

One concept in turbulence is the statistical approach and the reasoning in terms of wave numbers and cascading of energy and enstrophy as developed by Kolmogorov and others (see e.g. the review of [20]). This approach has been applied to the two–dimensional case by Kraichnan [27] and Batchelor [5] who predicted an energy spectrum proportional to k^{-3}. In [28] different numerical computations are reviewed part of which are in accordance with this prediction, most of which are not, however. The disagreement with respect to the statistical theory is attributed to the intermittency of the turbulent flow in these cases [3], an aspect which is not accounted for by the statistical theory.

In fact, a second concept in turbulence research is based on reasoning in physical space considering a vortex or coherent structure as the relevant entity. [2] and [43] proved that coherent structures substantially modify the cascading of energy. Scrambling the phase of the Fourier coefficients, which does not modify the spectrum but only destroys the coherent structures, reinstalls the decay rate predicted by the theory. This type of study suggested to consider the evolution of coherent vortices separately from a surrounding background with statistical behaviour. In [2] [6] thresholding of the vorticity was employed to accomplish such a separation and it was proved that the background indeed has a k^{-3} spectrum. Other criteria for the characterization have been developed in [44] and used for an automated census of vortices in order to obtain quantitative results for their behaviour.

Considering coherent structures as the dynamically active elements in a turbulent flow one could try to represent turbulent flow which is a continuous system with a reduced number of these physically motivated degrees of freedom. At this point, and also for later clarity, it is indicated to recall the difference of such an approach with respect to the proper orthogonal decomposition (POD) developed by Lumley [31]. Based on a statistical approach the POD aims, by means of the Karhunen–Loeve construction, at representing the whole ensemble of statistical events with few degrees of freedom. This yields optimality for the average. In contrast, extracting the coherent structures yields an optimal representation for one particular realization of the turbulent flow. The difference is also obvious by the fact that computing the coefficients of the POD for given statistics is a linear process while determining a representation in terms of

(approximate) coherent structures is non–linear.

The development of wavelets in the beginning of the 80ies had and still has a large impact on research in turbulence. This theory gives a unified framework for similar ideas which have been present long before such as shell models [45], [19] and wavepacket eddies [40]. Wavelets are characterized by simultaneous localization in space (or time) and frequency and by scale invariance. Hence, they may incorporate elements of both concepts cited above, coherent structures in physical space and cascades in frequency space.

Starting point for turbulence analysis by wavelets was the application to one–dimensional experimental time signals [29] and the analysis of two– and three–dimensional experimental and numerical flow fields [17], [15], [34]. Since then a lot of research in this direction has been carried out. Local quantities have been defined like local wavelet spectra [11] and local Reynolds number [15], [34], the fractal behaviour of turbulence has been examined. Other papers use wavelets for the efficient generation of turbulent signals with multiscale behaviour [12]. For an overview on existing wavelet techniques for turbulence we refer to [13], [16] and [1]. Numerical experiments as e.g. in [14] have shown that using the compression property of wavelets applied to the vorticity yields an efficient technique for separating coherent parts of the flow field from passive components. It thus improves the earlier approaches cited above and is the main motivation to use wavelets bases for the computation of turbulent flows.

Since the beginning, the subject of wavelets has considerably broadened. We now know redundant transforms, discrete wavelet bases, orthogonal, semi–orthogonal, non–orthogonal ones, and many other related constructions. For each application, also in turbulence, the appropriate variant has to be chosen. The above remarks were mainly concerned with physical reasoning. Independently, rephrasing the ideas of hierarchy, scale invariance, and localization in mathematical terms has also advanced the study of the Navier–Stokes equations in theoretical direction, i.e. proofs of existence and uniqueness [18], [8]. Another point of view relevant for the present work is the algorithmic aspect. Hierarchies and recursions yield fast algorithms. Due to the dual localization, differential and integral operators have a sparse representation in typical wavelet bases. This is exploited in several wavelet algorithms for the solution of PDEs (see e.g. the classification in [23]). Our objective therefore is to merge both aspects, the physical and the algorithmic one by directly computing turbulence in an adaptive wavelet basis. To our knowledge the present method is one of the first to accomplish this. Here, wavelets are employed rather close to the physical concepts mentioned above. This is due to the explicit representation of the vorticity in terms of a sum of wavelet functions. Preliminary results have been reported in [24]. Another approach coming more from the algorithmic side is the method developed by Perrier and Charton [9]. Therein, the starting point is a finite difference scheme on a regular cartesian grid, and wavelets are used at several stages to speed up the solution procedure by wavelet compression.

In the present paper we consider three different algorithms and apply them to calculate the same turbulent flow. The first is a classical pseudo–spectral Fourier method serving

as a reference. Second, we investigate the effect of wavelet compression during the evolution by supplementing the Fourier method with this feature. The third and main part is constituted by the adaptive wavelet discretization and its application. The numerical algorithm will be described only in its main elements here. Instead, we rather focus on the results and their analysis in physical terms. The proposed approach extends the use of wavelets from a posteriori analysis of computational results or experiments to directly computing in such a basis. This constitutes an important step for the application of wavelets to turbulence.

2 Physical problem

Let us consider the two–dimensional Navier–Stokes equations in vorticity–velocity formulation

$$\begin{aligned} \partial_t \omega + \mathbf{v} \cdot \nabla \omega - \nu \nabla^2 \omega &= 0 && (2.1) \\ \nabla \times \mathbf{v} &= \omega && (2.2) \\ \nabla \cdot \mathbf{v} &= 0 && (2.3) \end{aligned}$$

supplemented with initial and boundary conditions. Here, ω is the vorticity and $\mathbf{v} = (u, v)$ is the velocity field. Throughout we use dimensionless units. The computational domain is $\Omega = [0, 2\pi]^2$ with coordinate $\mathbf{x} = (x, y)$ and the flow is supposed to be periodic in both dimensions. The above equations are not modified further e.g. by the introduction of a hyperviscosity [4]. Since no external driving force is present an initially turbulent flow field asymptotically decays. Small vortices of equal sign merge to larger and larger vortices with filament–like structures between them (see e.g. [44] for a quantitative study of this process). In [32] it has been shown that the final state of such a numerical simulation with periodic conditions consists of two counter–rotating vortices which attenuate.

Using (2.2),(2.3) the velocity can, up to an additive constant, directly be expressed in terms of the vorticity

$$\mathbf{v} = \left(\frac{-\partial_y}{\partial_{xx} + \partial_{yy}} \omega \, , \frac{\partial_x}{\partial_{xx} + \partial_{yy}} \omega \right) \, . \tag{2.4}$$

The energy per unit mass of the system is

$$E(t) = \frac{1}{2} \frac{1}{4\pi^2} \int_\Omega \mathbf{v}^2(\mathbf{x}, t) \, d\mathbf{x} \tag{2.5}$$

and the specific enstrophy is

$$Z(t) = \frac{1}{2} \frac{1}{4\pi^2} \int_\Omega \omega^2(\mathbf{x}, t) \, d\mathbf{x} \, . \tag{2.6}$$

Some classical results for two–dimensional periodic flows are [20]

$$d_t E = -2 \, \nu \, Z \qquad , \qquad d_t Z = -2 \, \nu \, P \tag{2.7}$$

with the palinstrophy defined in this case by

$$P(t) = \frac{1}{2}\frac{1}{4\pi^2}\int_\Omega \mid \nabla\omega \mid^2 d\mathbf{x} \tag{2.8}$$

The quantity $W = \sqrt{Z/E}$ is the mean square wave number measuring the inverse average vortex size in a flow. It is bounded from below by 1 corresponding to structures of the size of the periodic domain. For two–dimensional flows one can show [33] that $d_t(W^2) \leq 0$, i.e. the average vortex size is monotoneously increasing.

Under periodic conditions the unknowns can be expressed in terms of their Fourier transform

$$\omega(\mathbf{x}) = \sum_{k\in\mathbb{Z}^2} \widehat{\omega}(\mathbf{k})\, e^{i\,k.x} \qquad , \qquad \widehat{\omega}(\mathbf{k}) = \frac{1}{4\pi^2}\int_\Omega \omega(\mathbf{x})\, e^{-i\,k.x} d\mathbf{x} \tag{2.9}$$

where $\mathbf{k} = (k_x, k_y)$ is the wave vector. Defining $\mathbf{k}^\perp = (-k_y, k_x)$, equation (2.4) reads

$$\mathbf{v}(\mathbf{x}) = \sum_{k\in\mathbb{Z}^2\setminus\{(0,0)\}} \frac{\mathbf{k}^\perp}{\mid \mathbf{k} \mid^2}\, \widehat{\omega}(\mathbf{k})\, e^{ik.x}\,. \tag{2.10}$$

Fourier transformation leads to the definition of an energy spectrum

$$E(k) = \frac{1}{2} \sum_{k-\frac{1}{2}<\mid k\mid\leq k+\frac{1}{2}} \mid \widehat{\mathbf{v}}(\mathbf{k}) \mid^2 \qquad , \qquad \mathbf{k}\in I\!N \tag{2.11}$$

and an enstrophy spectrum

$$Z(k) = \frac{1}{2} \sum_{k-\frac{1}{2}<\mid k\mid\leq k+\frac{1}{2}} \mid \widehat{\omega}(\mathbf{k}) \mid^2 \qquad , \qquad \mathbf{k}\in I\!N \tag{2.12}$$

which are related through $Z(k) = k^2 E(k)$. The specific energy and enstrophy, E and Z, are obtained by summation over all wave numbers k.

Theoretical results on two–dimensional turbulence are sumarized e.g. in [28]. We just recall here that according to [27], [5] there exists an enstrophy cascade leading by dimensional arguments to an energy spectrum $E(k) \sim k^{-3}$ while the energy is transfered from large wave numbers towards small wave numbers (in contrast to three–dimensional turbulence). However, it is not totally clear to what extent these results can be applied to the case of decaying turbulence since such flows are not statistically stationary [39], [32]. In a numerical computation of a decaying flow field furthermore the encountered energy spectrum depends on the initial condition. But even if the initial condition is chosen to exhibit a k^{-3} spectrum, direct numerical simulations generally produce a steeper decay [3],[42],[6]. This deviation is amply discussed in [7], [39], [43] where it is attributed to the presence of coherent vortices.

Since in the present flow the characteristic velocity is not constant due to the decay of the turbulence, the viscosity ν instead of a Reynolds number has been used to formulate the equations (2.1). All computations were done with $\nu = 2\cdot 10^{-3}$. Another frequently used quantity is the eddy turnover time $t_e = 1/\sqrt{2\,Z}$.

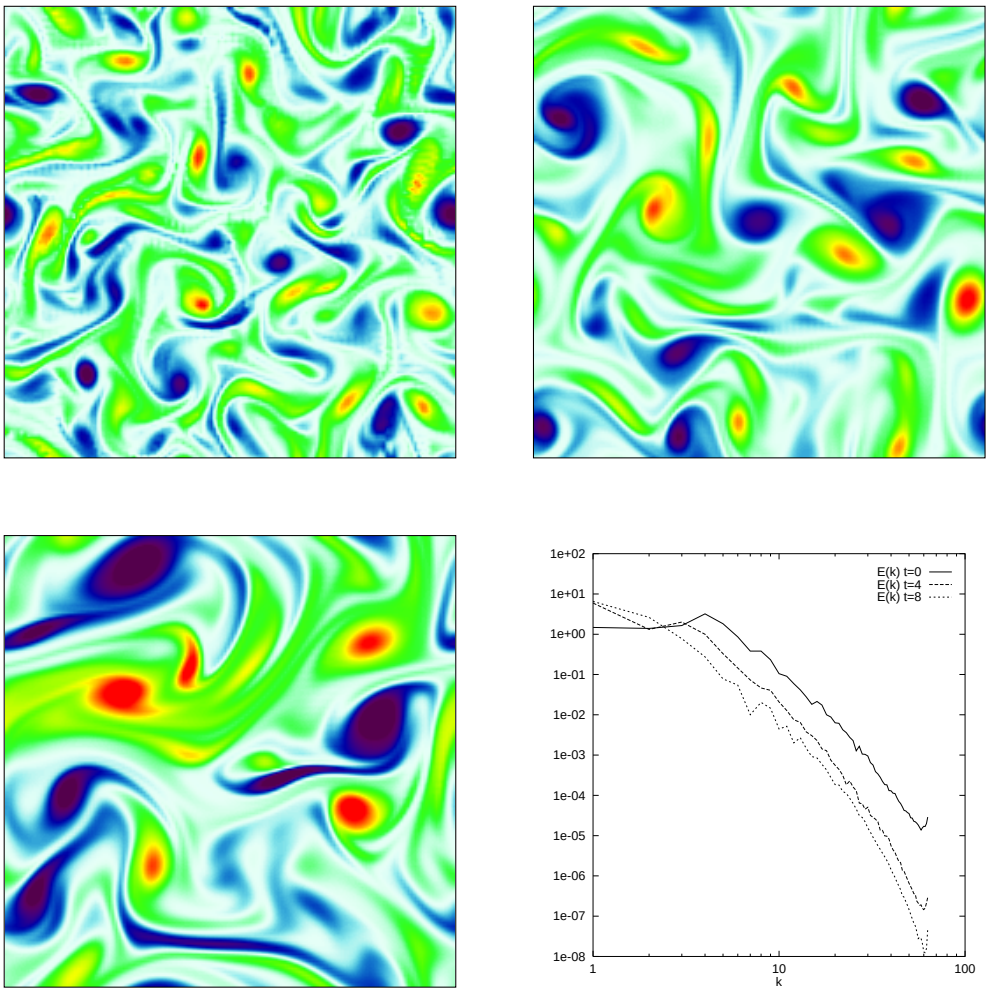

FIG. 1. Pseudo–spectral reference method. TOP: Vorticity field at $t = 0$, $t = 4$. BOTTOM: Vorticity at $t = 8$, Energy spectra at $t = 0, 4, 8$.

3 PSEUDO–SPECTRAL METHOD

We have implemented a classical pseudo–spectral Fourier method as described e.g. in [37]. It firstly serves as a reference method and second is employed for the generation of a suitable initial flow field as described below.

3.1 TIME SCHEME AND SPACE DISCRETIZATION

The employed time discretization is a semi–implict scheme of second order made up of a BDF formula for the viscous term and an Adams–Bashforth extrapolation for the convection term. It reads

$$(\gamma - \nu\nabla^2)\omega^{n+1} = \frac{4}{3}\gamma\omega^n - \frac{1}{3}\gamma\omega^{n-1} - \mathbf{v}^* \cdot \nabla\omega^* \tag{3.1}$$

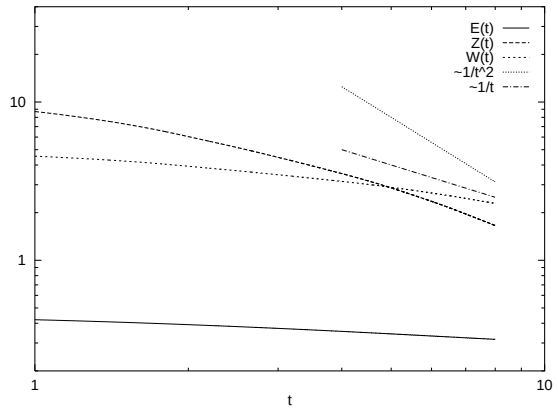

FIG. 2. Spectral Fourier computation. Evolution of energy E, enstrophy Z, and average wavenumber W.

with $\gamma = 3/(2\Delta t)$, $\mathbf{v}^* = 2\mathbf{v}^n - \mathbf{v}^{n-1}$ and $\omega^* = 2\omega^n - \omega^{n-1}$. For start up a similar first order scheme is used. This scheme has been thoroughly tested in [41] and has found wide application for spectral methods. The same discretization has also been used in the algorithms presented below. In all computations the time step was $\Delta t = 10^{-3}$.

The Fourier discretization is based on the development (2.9) truncated at $k = -N/2$ and $k = N/2 - 1$. The velocity $\mathbf{v}$ and the gradient of ω are computed in Fourier space by means of (2.10) and by multiplication with $i\mathbf{k}$, respectively. The convection term is then evaluated by the pseudo–spectral technique in physical space without dealiasing.

3.2 Initial condition

For the computation of decaying turbulence it is classical to use an initial condition which has a spectrum close to the statistically steady case. We generated such a flow field as described in [36] using Gaussian random numbers which allows to impose an arbitrary energy spectrum of the initial state. We used the broad band spectrum

$$E(k) = c\frac{k^2}{k_0^6 + k^6}e^{-k^2/k_\nu^2} \tag{3.2}$$

for $k \leq k_f$ and $E(k) = 0$ for $k > k_f$ with $k_0 = 10$, $k_\nu = 40$, $k_f = 42$, and the constant c chosen to give $E = 1/2$ [26]. The wave numbers k_0 and k_ν would correspond in a stationary case to the wave number at which energy is injected and dissipated, respectively. A suitable vorticity field to start the later computations is obtained by using this state as initial condition and computing its evolution during a certain laps of time, here during $T_{init} = 2$ equal to about 8 initial eddy turnover times. The resulting solution is well resolved and exhibits a smooth spectrum with the desired decay (see Fig.1). It is used as initial condition for all the subsequent computations and is therefore assigned the time $t = 0$.

3.3 Results of the pseudo–spectral computation

Starting from the solution at $t = 0$ generated as described above we calculated the evolution of the flow up to $t = 8$. The vorticity field at $t = 0$, $t = 4$, and $t = 8$ is reported in Fig.1. The colour scale has been adjusted to account for the decrease in amplitude and is the same for all subsequent pictures at a certain time.

It is obvious that in the course of time small vortices of equal orientation merge to larger and larger ones. Coherent structures consisting of counter–rotating vortex pairs form and become more and more pronounced. We also observe the rolling up of sheet–like filaments around centers of vorticity concentration which is typical for such flows.

The energy spectra corresponding to the vorticity fields are also reported in Fig.1. The energy at large wave numbers decreases and at small wave numbers increases which is in accordance to the inverse energy cascade mentioned above. The enstrophy spectrum behaves similarly without such an increase according to the enstrophy cascade. As in many references we also find a spectrum which is steeper than the one predicted by the theory of Kraichnan and Batchelor. The perturbation at the tail of the spectra could be avoided by de–aliasing. We decided not to use this feature here to allow for later comparison since it employs a finer grid not present in the wavelet computations.

Finally, we report the evolution of $E(t), Z(t)$, and $W(t)$ in Fig.2. The decrease of Z is stronger than the one of E which is in accordance to the fact that $d_t(W^2)$ is negative. At $t = 8$ the energy is 68% of its value at $t = 0$ while the enstrophy has decreased to 12%. Following [5] the decay of Z should be proportional to t^{-2}. However, our computations yield a rate between t^{-2} and t^{-1} which has also been observed in [33] and therein attributed to the temporal intermittency of the flow.

In summary we can state that the results of the Fourier pseudo–spectral method show the same behaviour as reported in recent literature. They can therefore be used as reference for the wavelet methods investigated below.

4 Pseudo–spectral method with wavelet compression

4.1 Wavelet basis and wavelet representation

4.1.1 Multiresolution

In this section we briefly recall some required notions and refer the reader to textbooks such as [35] for an exhaustive treatment of the theory of wavelets.

For ease of presentation we consider the two–dimensional 1–periodic torus $\mathbb{T}^2$ with $\mathbb{T} = \mathbb{R}/\mathbb{Z}$ which will for the applications be rescaled to $\Omega = [0, 2\pi]^2$. Let us start with the space of square–integrable functions on this domain $L^2(\mathbb{T}^2)$ with scalar product $\langle f, g\rangle = \int_{\mathbb{T}^2} f(x, y)\, g(x, y)\, dx\, dy$ and norm $\|f\|_2^2 = \langle f, f\rangle$. A multiresolution analysis (MRA) of this space consists of a ladder of imbedded subspaces $V_0 \subset V_1 \subset V_2 \subset \ldots$ with $\lim_{j\to\infty} V_j = L^2(\mathbb{T}^2)$ and V_0 containing only constant functions. Each of these

spaces V_j is spanned by regular shifts of a refinable function b_j,

$$V_j = span\{\ b_j(x - \frac{i_x}{2^j}, y - \frac{i_y}{2^j})\ \}_{i_x=0,\ldots,2^j-1, i_y=0,\ldots,2^j-1}\ . \tag{4.1}$$

If these translates are mutually orthonormal the function b_j is classically termed scaling function and denoted by ϕ_j. If b_j is interpolating, this function is a cardinal function and denoted by S_j with

$$S_j(\frac{k_x}{2^j}, \frac{k_y}{2^j}) = \delta_{k_x,0}\,\delta_{k_y,0} \qquad , \qquad k_x, k_y = 0, \ldots, 2^j - 1\ . \tag{4.2}$$

One way to construct a higher dimensional MRA is to employ the tensor product of the equivalent functions in a one–dimensional MRA [35]. In the present two–dimensional case this means

$$\phi_j(x, y) = \tilde{\phi}_j(x)\,\tilde{\phi}_j(y) \qquad , \qquad S_j(x, y) = \tilde{S}_j(x)\,\tilde{S}_j(y) \tag{4.3}$$

where $\tilde{\phi}_j$ and $\tilde{S}_j$ are the scaling function and the cardinal function of a one–dimensional MRA, respectively.

Due to the periodicity constraint the usual scale invariance only holds approximately, i.e.

$$\phi_{j+1}(x, y) \approx 2\phi_j(2x, 2y) \qquad , \qquad j >> 0 \tag{4.4}$$

with equality obtained in the limit $j \to \infty$. Instead, exact recursions hold in Fourier space

$$\widehat{\phi}_{j,n_x,n_y}(k_x, k_y) = 2\ e^{-2\,\pi\,i\,(k_x n_x + k_y n_y)/2^j}\,\widehat{\phi}_{j+1,0,0}(2k_x, 2k_y) \qquad , \qquad (k_x, k_y) \in \mathbb{Z}^2, j \geq 0. \tag{4.5}$$

4.1.2 Wavelets

An essential feature of the wavelet representation is to work with the orthogonal complement spaces $W_j = V_{j+1} \ominus V_j$. These spaces are generated by regular shifts of wavelet functions. For the present tensor product construction (4.3) V_j has 2^{2j} degrees of freedom, hence W_j has 3.2^{2j}. It can be shown [35] that three different wavelets are necessary to span W_j by shifts of 2^{-j} in x and y. They read

$$\psi^{\varepsilon}_{j,i_x,i_y}(x, y)\ =\ \begin{cases} \tilde{\psi}_{j,i_x}(x)\ \tilde{\phi}_{j,i_y}(y) & ;\ \varepsilon = 1 \\ \tilde{\phi}_{j,i_x}(x)\ \tilde{\psi}_{j,i_y}(y) & ;\ \varepsilon = 2 \\ \tilde{\psi}_{j,i_x}(x)\ \tilde{\psi}_{j,i_y}(y) & ;\ \varepsilon = 3 \end{cases} \tag{4.6}$$

with $j \geq 0$ and $i_x, i_y = 0, \ldots 2^j - 1$. Here, $\tilde{\psi}_j$ is the wavelet corresponding to the one–dimensional MRA generated by the functions $\tilde{\phi}_j$. Similar to (4.4) scale invariance only holds approximately in physical space but is replaced by recursions in Fourier space resulting from (4.5).

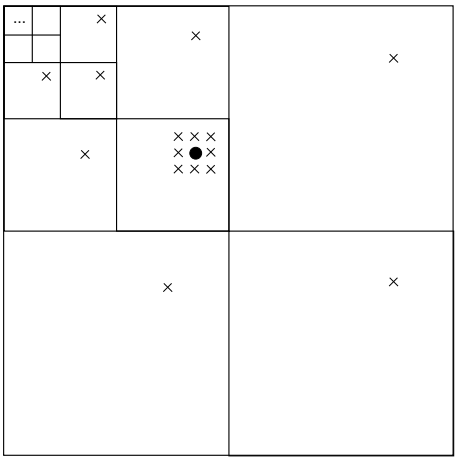

FIG. 3. Representation of the wavelet coefficients for a two–dimensional MRA and illustration of the applied neigbouring relation. The crosses and the dot designate the set $N(\lambda)$ with the dot representing the index λ.

The above orthogonal decomposition $L^2(\mathbb{T}^2) = V_0 \oplus_{j\geq 0} W_j$ can be used to represent any function $f \in L^2(\mathbb{T}^2)$ as

$$f(x,y) \;=\; c_{0,0,0}\,\phi_{0,0,0}(x,y) \;+\; \sum_{j\geq 0}\sum_{i_x=0}^{2^j-1}\sum_{i_y=0}^{2^j-1}\sum_{\varepsilon=1}^{3}\; d^{\varepsilon}_{j,i_x,i_y}\;\psi^{\varepsilon}_{j,i_x,i_y}(x,y) \qquad (4.7)$$

where $\phi_{0,0,0} = 1$. Recall that in the classical case all elements of the employed basis $\{1, \psi_{j,i_x,i_y}\}$ are mutually orthonormal with respect to the L^2 scalar product. Consequently the coefficients in (4.7) are $c_{0,0,0} = \int_{\mathbb{T}^2} f(x,y)\,dx\,dy$ and $d^{\varepsilon}_{j,i_x,i_y} = \langle u,\ \psi^{\varepsilon}_{j,i_x,i_y}\rangle$. In all computations below we employ exponentially decaying cubic spline wavelets. Hence, $\tilde{S}_j$ is the periodic two–dimensional cardinal spline function with knot spacing $1/2^j$. The functions $\tilde{\psi}$ and $\tilde{\phi}$ are the Battle–Lemarié spline wavelet and the corresponding scaling function periodized as described in [38], [35]. For detailed graphical illustration we refer to [11].

4.1.3 Wavelet transform

The practical computation of the wavelet representation (4.7) has to be restricted to some $f_J \in V_J$ with the sum over j extending only up to $J-1$. In general no restriction is applied to the shift indices i_x, i_y (see Section 5 for this feature in an adaptive discretization). If all coefficients for $j = 0, \ldots, J-1$ are to be computed the usual way is to start from given values f_{i_x,i_y} at the points $(\frac{i_x}{2^J}, \frac{i_y}{2^J})$. The function f_J is then defined by a collocation projection imposing $f_J(\frac{i_x}{2^J}, \frac{i_y}{2^J}) = f_{i_x,i_y}$. Subsequently the classical Mallat algorithm is employed to first determine the coefficients $d^{\varepsilon}_{J-1,i_x,i_y}$ and the remainder of f_J which is in V_{J-1}. The latter contribution is decomposed again to determine the

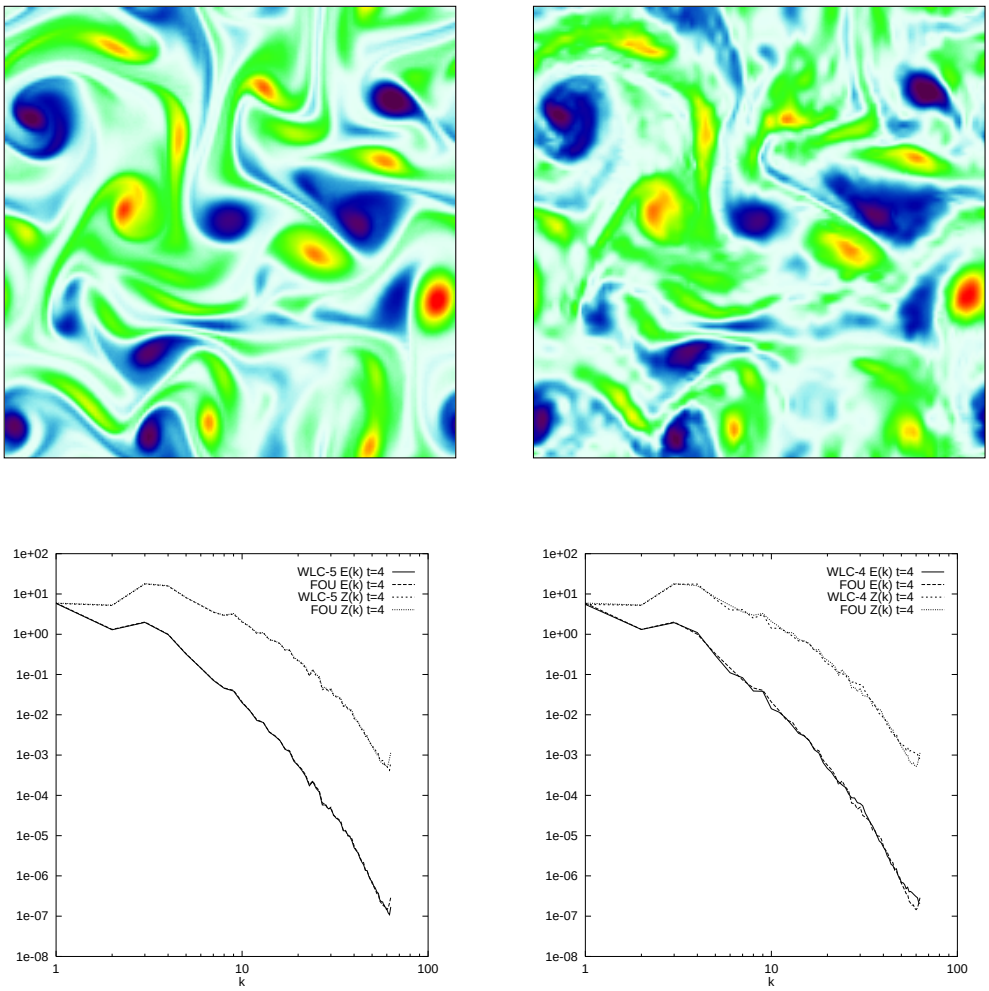

FIG. 4. Pseudo–spectral Fourier method with wavelet compression in each time step. Solution at $t = 4$ with $\epsilon = 10^{-5}$ (left) and $\epsilon = 10^{-4}$ (right). TOP: Vorticity fields. BOTTOM: Spectra of energy and enstrophy.

coefficients $d^{\varepsilon}_{J-2,i_x,i_y}$ and so on down to $j = 0$. Due to the constant shifts of $1/2^j$ on each level j and the periodicity of f_J and all its components in (4.7) the computations are most conveniently executed by FFT (cf. remarks in [21]). This is no longer the case for an adaptive wavelet basis as used in Section 5. The inverse transform which consists in determining the values $f_J(\frac{i_x}{2^j}, \frac{i_y}{2^j})$ from the coefficients in (4.7) proceeds in reversed order, again via fast convolutions by FFT.

4.1.4 Graphical representation of the coefficients

Let us finally recall a widely applied scheme for the representation of wavelet coefficients in two dimensions. The amplitude of $d^{\varepsilon}_{j,i_x,i_y}$ is positioned at the point (x, y) with $x = 2^j(1 - \delta_{\varepsilon,3}) + i_x$ and $y = 2^j(1 - \delta_{\varepsilon,1}) + i_y$. Fig.3 illustrates the resulting diagram. The lines separate regions with different j and different ε. The square in the lower right

corner contains the coefficients of the "diagonal wavelets" on the finest scale, d^3_{J-1,i_x,i_y}. The square above it contains the "horizontal coefficients" of the same scale, those with $\varepsilon = 1$, and the square left of it the "vertical coefficients" of this scale with $\varepsilon = 2$. The next smaller boxes contain the coefficients of scale $J-2$ in a similar manner and so forth.

4.2 Wavelet compression

The orthogonality of the wavelet basis introduces an intimate relation between the L^2–norm of a function f and its wavelet coefficients

$$\|f\|_2^2 = (c_{0,0,0})^2 \; + \sum_{j\geq 0} \sum_{i_x=0}^{2^j-1} \sum_{i_y=0}^{2^j-1} \sum_{\varepsilon=1}^{3} (d^{\varepsilon}_{j,i_x,i_y})^2 \tag{4.8}$$

Other equivalences relating a certain norm to the wavelet coefficients can be obtained by weighting the latter in a different way [35]. Hence, modifying a coefficient in a wavelet expansion, e.g. by setting it to zero, can directly be related to the resulting difference in the norm. Leaving out small coefficients in (4.7) will therefore only introduce a minor error of f with respect to the L^2–norm. Wavelet compression of data or a function aims at determining a good approximation with a small number of degrees of freedom: Starting from a function f the projection onto f_J and wavelet decomposition are executed as described above. Next, all coefficients with absolute value smaller than some prescribed tolerance ϵ are eliminated. The resulting coefficients correspond to a function close to f but generally with highly reduced storrage cost. Let us mention that there exists a well–developed theory relating the linear and non–linear approximation of a function in terms of wavelets to the global and local smoothness of this function [35],[10]. For practical use these results can however only give qualitative hints as they are concerned with the asymptotic behaviour for $j \to \infty$.

An important property of the functions ψ is their simultaneous localization in space and frequency. Consequently, the coefficient $d^{\varepsilon}_{j,i_x,i_y}$ monitors the oscillation of f with frequency around $\xi = 2^j$ near the point $(i_x/2^j, i_y/2^j)$ – horizontal, vertical or diagonal according to ε (cf. the illustration in [11]). In terms of wavelet representation and compression we can therefore retain that any action on a coefficient, e.g. its elimination, has only local effect in space and frequency which is in contrast to the Fourier representation. It allows to distinguish between coherent structures and intermediate filaments whereby accounting for intermittency of a flow is possible.

4.3 Computational approach

In [14] it has been conjectured that the dynamically active structures in a turbulent flow correspond to the large wavelet packets coefficients while the passively advected part of the flow is represented by the remaining small coefficients. The use of wavelet packets instead of wavelets in this reference is of minor importance (recall that wavelets are a subset of wavelet packets). The two parts have been separated in an initial

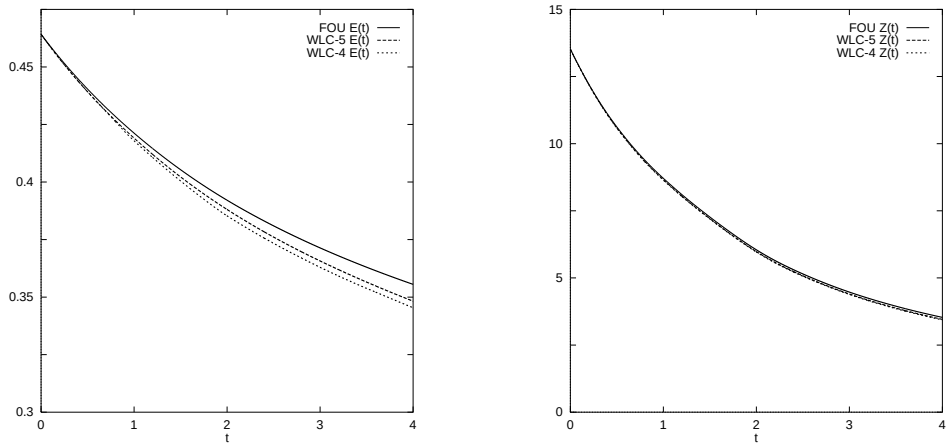

FIG. 5. Wavelet compression in each time step. Evolutions obtained with $\epsilon = 10^{-4}$, $\epsilon = 10^{-5}$, and $\epsilon = 0$ (reference). LEFT: Energy. RIGHT: Enstrophy.

turbulent flow field with different compression rates. Then the evolution with and without the presence of active and passive components has been studied employing a pseudo–spectral method similar to the one described in Section 3. By comparison it has been shown that the wavelet packet representation is much more adapted to the physics of turbulence than the Fourier basis because of its locality in space. It can account for the concentration of vorticity in small parts of the domain which is characteristic for the considered flows. However, the separation has been done only once, namely at the beginning of the evolution. The role of active and passive components at later stages could not be examined.

In Section 5 we shall present results obtained with an adaptive wavelet discretization computing only the large wavelet coefficients of the vorticity field. As an intermediate step we investigate the same flow with the Fourier method supplemented by a wavelet compression in each step: the pseudo–spectral method is applied as above, in each time step a wavelet transform is executed, coefficients smaller than the tolerance ϵ are eliminated before the solution is transformed back to physical space to continue with the next time step.

4.4 Results of wavelet–compressed pseudo–spectral method

The Fourier algorithm with wavelet compression has been applied to the initial condition used in Section 3.3. The resulting vorticity fields for tolerances $\epsilon = 10^{-5}$ and $\epsilon = 10^{-4}$ at time $t = 4$ are depicted in Fig.4. Comparing these with the results of the original Fourier method in Fig.1 ($\epsilon = 0$) we find good qualitative agreement. As expected the result is better for smaller ϵ. Let us also mention that with $\epsilon = 10^{-3}$ (not shown here) the dynamics of the flow are lost. The spectra of energy and enstrophy are reported as well in Fig.4. Although for larger k the difference with respect to the uncompressed computation becomes visible the spectra do not exhibit substantial deviations from the

reference solution. As in each time step the wavelet coefficients of the vorticity below the prescribed tolerance are set to zero it is not astonishing that enstrophy is lost in the course of time. In Fig.5 we therefore also represent the evolution of energy and enstrophy. At $t = 4$ a deviation from the Fourier computation of -2.1% and -2.7% is observed with $\epsilon = 10^{-5}$ and $\epsilon = 10^{-4}$, respectively. Also for the energy $E(t)$ the behaviour is qualitatively the same yielding a relative difference of -2.1% and -2.9% at $t = 4$ in these computations.

The above results constitute a further step with respect to [14] where only the initial state of the turbulent flow field has been compressed. In the present study wavelet compression is repeated in each time step. We show that the conclusion of [14] remains valid and that the essential dynamics of the turbulent flow field are represented by the strong wavelet coefficients of the vorticity.

4.5 Conservation properties

The elimination of enstrophy during the compression step – although it remains very small – raises the question of a possible cure to this unphysical loss. This, however, would require a means for "re–injecting" the enstrophy which is represented by the neglected coefficients into the retained ones. It amounts to devising a model which in some sense realizes a sort of forcing for the flow. Since there is a large variety of possible choices which requires detailed investigation we did not attempt to implement such a device here. Studies concerned with forcing in wavelet coefficients space to obtain a statistically stationary turbulent flow are currently under way and seem to be promissing, but this topic is beyond the scope of the present paper.

5 Adaptive wavelet discretization

5.1 Numerical Scheme

In Section 4 the wavelet representation has been described and wavelet compression of a function has been employed to compress ω^{n+1} in each time step. In [21], [23] we have developed an adaptive discretization scheme for the sollution of elliptic PDEs and applied it to reaction–diffusion equations. With an appropriate semi–implicit time scheme this algorithm can now be extended to solve (2.1)–(2.2) directly in a wavelet basis. This amounts to restricting the full index range for $\lambda = (j, \varepsilon, i_x, i_y)$, $j < J$, denoted Λ_J, to some subset $\Lambda \subset \Lambda_J$. If the number of indices in Λ is smaller than $2^{j_{max}+1}$, where j_{max} is the finest scale in Λ, the elements designated by Λ are termed 'lacunary basis'. In an adaptive method the set Λ generally is of this type and changes in time. Hence, at each time step n the vorticity is represented as

$$\omega^n(x, y) = \sum_{\lambda \in \Lambda^n} d_\lambda^n \, \psi_\lambda(x, y) \tag{5.1}$$

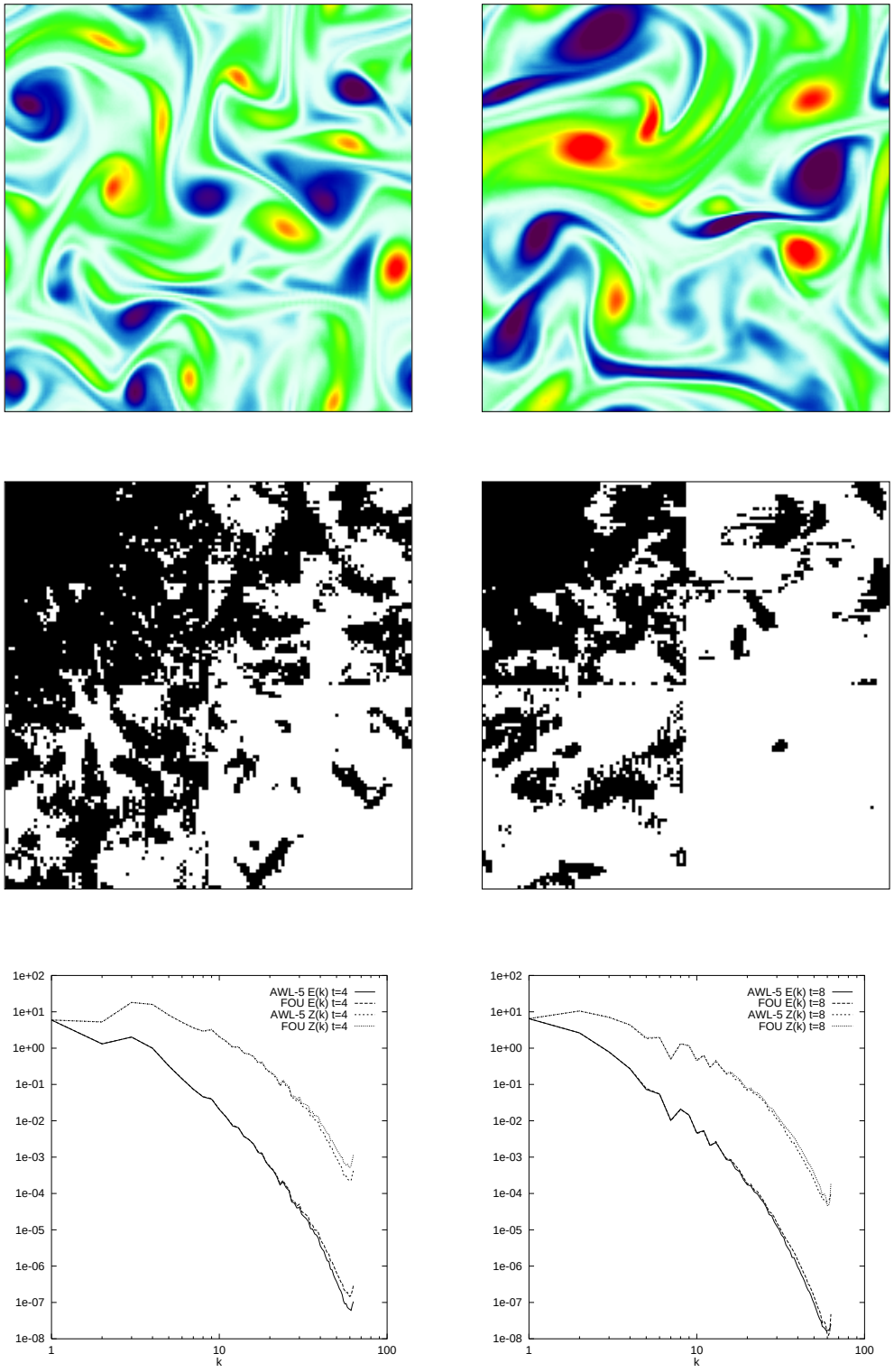

FIG. 6. Adaptive wavelet method with $\epsilon = 10^{-5}$. Solution at $t = 4$ (left), $t = 8$ (right). TOP: Vorticity fields. MIDDLE: Active wavelet coefficients. BOTTOM: Comparison of the energy spectra to those obtained with the pseudo–spectral method.

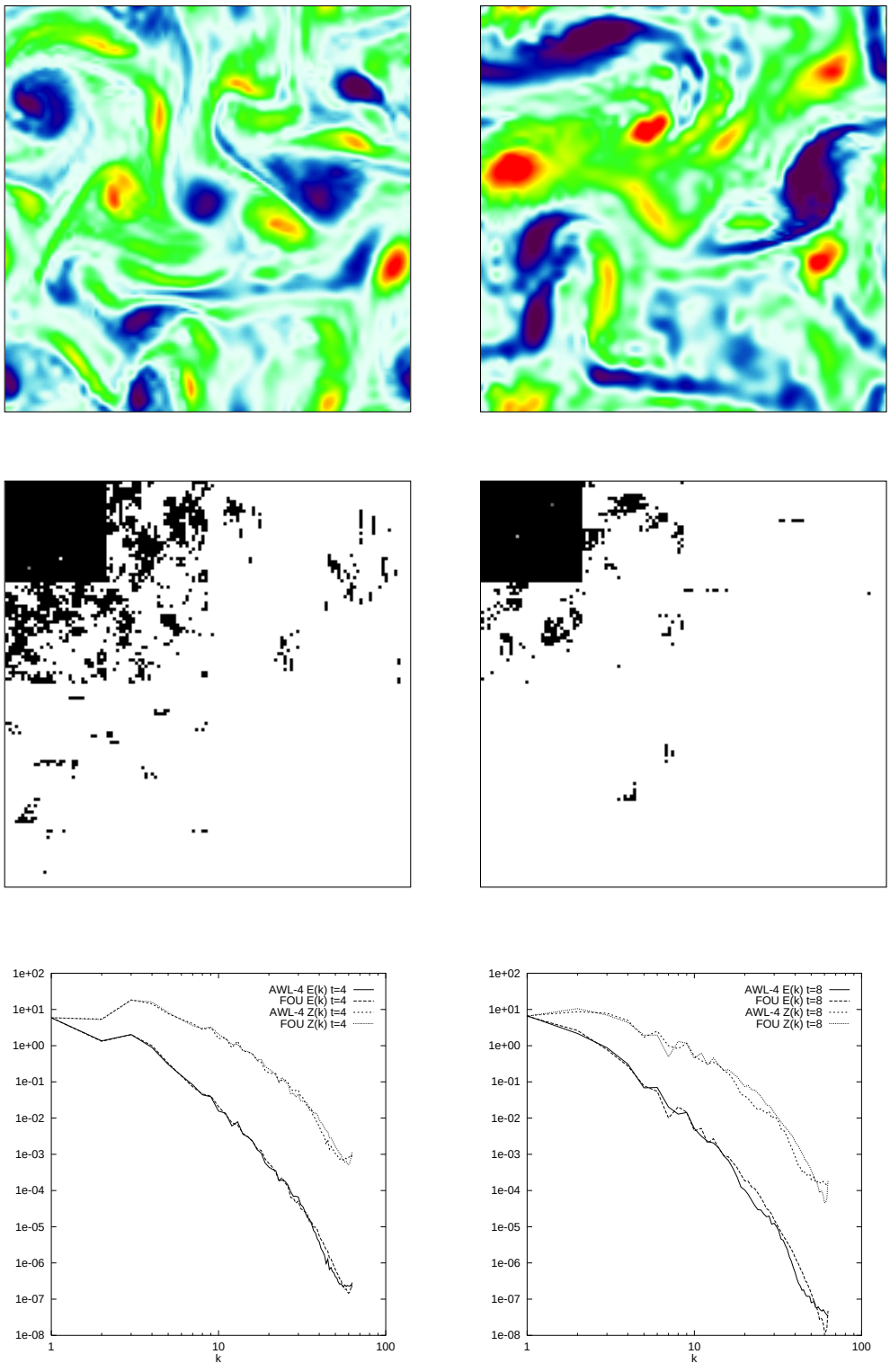

FIG. 7. Adaptive wavelet method with $\epsilon = 10^{-}4$. Solution at $t = 4$ (left), $t = 8$ (right). TOP: Vorticity fields. MIDDLE: Active wavelet coefficients. BOTTOM: Comparison of the energy spectra to those obtained with the pseudo–spectral method.

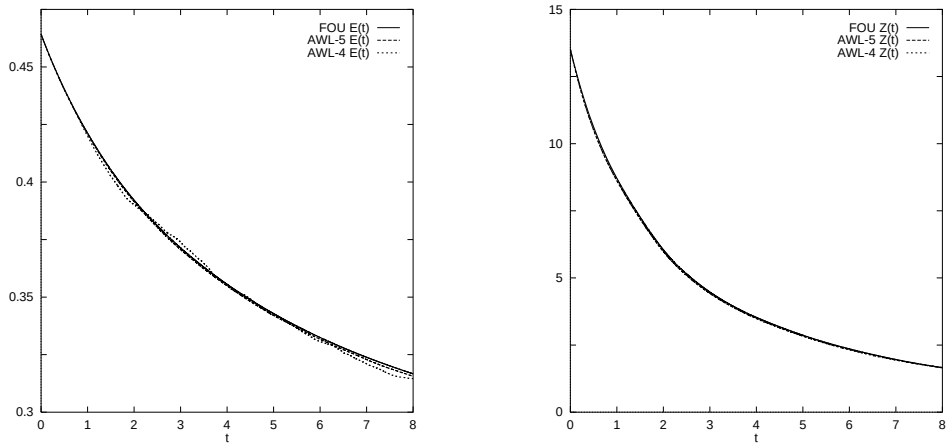

FIG. 8. Adaptive wavelet computations with $\epsilon = 10^{-4}$ and $\epsilon = 10^{-5}$. LEFT: Evolution of energy. RIGHT: Evolution of enstrophy.

with the appropriate adjustments to include the coefficient $c_{0,0,0}$ in this sum. In fact for the present application this contribution can be disregarded if initially zero.

From the algorithmic point of view an adaptive numerical discretization of a PDE has to contain the following elements:

(i) error estimation.

(ii) adaption of the discretization according to (i).

(iii) assembly of the system to be solved.

(iv) solving for the unknowns.

Part (i) and (ii) are implemented in a way which has become classical for wavelets [30], here extended to two dimensions. Starting from a representation with index set Λ^n (at $t = 0$ this is the full set) those coefficients with $\mid d_\lambda \mid < \epsilon$ are eliminated to generate a set Λ^* containing the remaining indices. The index set for the next time step Λ^{n+1} is then made up of the union of the set of neighbours $N(\lambda)$ (also containing λ itself) with $\lambda \in \Lambda^*$. The set N can be chosen in different ways. We used a definition obtained by modifying each of the indices j, ε, i_x, i_y by one as illustrated in Fig.3. The coefficients with indices in Λ^{n+1} are then to be computed. This procedure ressembles blow up and skeleting in image processing and allows to follow an unsteady solution. Furthermore, assuming the usual (asymptotic) decay of the wavelet coefficients, as e.g. known for differentiable functions, an estimate of the discretization error in space can be obtained by means of the coefficients in $\Lambda^n \setminus \Lambda^*$.

Let us now consider the elements (iii) and (iv) of the algorithm. In each time step eq. (3.1) has to be solved for ω^{n+1} represented according to (5.1). For simplicity we write

$L = \gamma - \nu \nabla^2$ and designate the r.h.s. of (3.1) by f. A Petrov–Galerkin method with trial functions ψ_λ and test functions θ_λ then yields

$$\sum_{\lambda \in \Lambda^{n+1}} d_\lambda^{n+1} \, \langle L \, \psi_\lambda, \theta_{\lambda'} \rangle = \langle f, \theta_{\lambda'} \rangle \qquad , \qquad \forall \lambda' \in \Lambda^{n+1} \; . \tag{5.2}$$

Requiring a sufficient number of vanishing moments for the functions ψ_λ (recall that by definition a wavelet has at least one vanishing moment) allows to define $\theta_\lambda = (L^{-1})^* \psi_\lambda$ [30] and determine these in a stable way. With this choice of test and trial functions the matrix on the l.h.s. of (5.2) reduces to the unit matrix due to the orthogonality of the wavelet basis. Hence, step (iv) becomes trivial.

The remaining step (iii) with the computation of the scalar products $\langle f, \theta_{\lambda'} \rangle$ is the most difficult one due to the restriction of λ to Λ^{n+1}. A truely adaptive method is characterized by the fact that the coefficients d_λ are not computed for $\lambda \notin \Lambda^{n+1}$ (and subsequently canceled). This excludes the use of FFT as employed in Section 4 and raises technical difficulties. In [22], [23] we have devised and analyzed a hierarchical algorithm for the computation of the coefficients in a lacunary wavelet basis. It is based on the bi–orthogonal operator–adapted functions θ_λ and $\mu_\lambda = L\psi_\lambda$. The later generate a MRA of which the cardinal function is used to accomplish the decomposition. It makes use of hierarchical collocation on partial grids with spacing $1/2^j$ successively coarsening from $j = J$ down to $j = 0$. The algorithm has linear operation count which results from the truncation of the involved filters to finite length. This in turn is possible due to the localization of the wavelets as well as the other deduced functions in physical space.

In summary one time step consists of the following operations (the required filters being computed in pre–processing):

0. given coefficients d_λ, $\lambda \in \Lambda^n$.

1. determine Λ^{n+1} via Λ^*.

2. determine the quadrature points required for the later evaluation of $\langle f, \theta_{\lambda'} \rangle$.

3. inverse adaptive wavelet transform to determine ω^n at these points.

4. evaluation of the r.h.s. f at the quadrature points.

4. computation of $d_\lambda^{n+1} = \langle f, \theta_{\lambda'} \rangle$.

Further details and analysis can be found in the cited references. Let us mention that at present the non–linear term in the r.h.s. of (3.1) is evaluated by FFT using (2.10) and derivation in Fourier space. This will be modified in the near future.

5.2 Results of adaptive wavelet simulations

Starting from the same initial condition as used for the previous cases the evolution of the flow field has been computed by the adaptive wavelet method up to $t = 8$. As before we used tolerances $\epsilon = 10^{-4}$ and $\epsilon = 10^{-5}$ which were constant within each run.

For the initial condition the compression rate is not very high since a large number of coherent structures are present. The intermittency of this state is low. With both values of ϵ almost all of the 16384 possible degrees of freedom are retained at $t = 0$. As described and illustrated above the intermittency increases in the course of the evolution of the flow field. Hence, at later stages the number of active coefficients decreases and the impact of the adaptive wavelet representation becomes stronger.

Fig.6 shows the vorticity field obtained at $t = 4$ and $t = 8$ with $\epsilon = 10^{-5}$. The solution does not exhibit a visible difference with respect to the reference solution in Fig.1. The computed wavelet coefficients are depicted below the vorticity fields. At $t = 4$ their number is 8115, i.e. 50%, and at $t = 8$ it is 4723, i.e. 29%, respectively. The spectra $E(k)$ and $Z(k)$ which are represented as well do not show any significant difference compared to the reference values. Hence, all scales are well resolved with a reduced number of degrees of freedom.

In Fig.7 we represent the same graphics as in the previous figure, now obtained with $\epsilon = 10^{-4}$. Consequently less degrees of freedom are used, namely 2277 at time $t = 4$ and 1362 at $t = 8$, respectively. At $t = 4$ we still observe a good agreement between the computed solution and the reference run although only 11% of the full coefficient set are used. However, at $t = 8$ with 8% of the coefficients the dynamics of the flow are destroyed. The local structure of the vorticity exhibits differences, although the global structure is conserved. These observations are supported by the related spectra. They exhibit deviations in particular for high wave numbers, larger at $t = 8$ but still similar to the reference solution at $t = 4$.

Let us mention that the maximal resolution of 128^2 degrees of freedom in the present computations is fairly low. This limits the mean square wavenumber W or in other words the Reynolds number. Hence the turbulent fluctuations decay relatively fast leaving little time for the generation of intermittency during this process. Consequently the observed compression rates have to remain moderate. For larger Reynolds numbers, i.e. higher resolution, the impact of adaptivity will become more pronounced as can be infered from comparison of the reported vorticity fields to results obtained with higher resolution and/or hyperviscosity showing stronger intermittency of the flow, e.g. [25].

5.3 Evolution of energy and enstrophy

Complementary information to the figures discussed so far is given by the evolution of $E(t)$ and $Z(t)$ in Fig.8. The result of the Fourier computation is inserted for comparison. Similarly to the computations with wavelet compression we observe a loss in E and Z in the course of time. However, it is much smaller than for the pseudo–spectral method with wavelet compression. Taking e.g. the case with $\epsilon = 10^{-5}$ we recognize that at $t = 4$ the difference is only 0.17% in energy and 0.93% in enstrophy. At $t = 8$ these values are 0.28% and 0.45% for energy and enstrophy, respectively. A possible explanation of these results is that in contrast to the spectral method with wavelet compression the wavelet coefficients are now computed in an adaptive basis with locally refined grids for quadrature. We conjecture that the slight aliasing error introduced by the truncation

of the filters redistributes the enstrophy over the scales. On the other hand the initial "cloud" of coefficients is followed during the evolution without setting any coefficient to zero. If an index $\lambda \in \Lambda^n$ is not retained in Λ^{n+1} its coefficient is still present in the r.h.s. of the time stepping in our algorithm. Hence it might as well be that this procedure is responsible for the different behaviour. Another influence may stem from the difference in the cascades for both quantities. Enstrophy is transfered from small wave numbers to large wave numbers so that an error in representing the vorticity by the computed wavelet coefficients is transfered to large wave numbers as well where it goes into small coefficients and leaves the adaptive basis. On the contrary the cascade for energy is inverse so that errors committed on fine scales propagate to small wavenumbers and may accumulate. This point requires further investigation.

6 Conclusion

The method presented in this paper exploits the properties of wavelets in different ways. From the algorithmic point of view an adaptive wavelet discretization yields a sparse and economic representation of the solution. The hierarchy of the basis yields error estimations and hierarchical algorithms. Orthogonality and vanishing moments are a prerequisite for the employed test functions in the Petrov–Galerkin method. Of course, it would be convenient to have one single wavelet function instead of three, but constructions with all the required properties are currently not available.

The physical motivation for representing turbulent flow fields with pronounced coherent structures in terms of wavelets has been sketched in the introduction. The performed computations show that the extraction of coherent vortices is quite reliable – determined by only one parameter, the tolerance ϵ. Here, one might in the case of decaying turbulence also try to use a temporally varying value. The computations illustrate also how the active wavelet basis functions representing the vorticity field accumulate in the coherent structures, more precisely at locations where the spatial derivatives of ω are large. This is due to the vanishing moments of these functions. On the other hand, local gradients of the vorticity determine the local transfer of energy and enstrophy from scale to scale which is essential for turbulence.

The computations with a pseudo–spectral method and wavelet compression support this picture. Even when compressing the vorticity field in each single time step the turbulent dynamics are well captured provided that this is not done excessively. Of course, we do not advocate this approach for running large scale computations as it involves only losses in terms of precision and CPU time with respect to the pure pseudo–spectral method. Rather, its consideration is usefull in comparison to the adaptive wavelet method. In this new algorithm, only the required wavelet amplitudes are computed. Obviously their relative number reduces for increasing intermittency. Related studies with higher resolution and lower viscosity are currently under way. Further perspectives are the inclusion of new physical models such as forcing in wavelet space and the relation to shell models.

Acknowledgement: K.S. would like to acknowledge partial support through PROCOPE contract 95-137 "Méthodes particulaires, méthodes pseudo–spectrales et techniques d'ondelettes pour le traitement d'images et la mécanique des fluides".

References

[1] A. Arneodo, F. Argoul, E. Bacry, J. Elezgaray, and J. Muzy. *Ondelettes, Multifractals et Turbulence.* Diderot Editeur, 1995.

[2] A. Babiano, C. Basdevant, B. Legras, and R. Sadourny. Vorticity and passive-scalar dynamics in two–dimensional turbulence. *J. Fluid Mech.*, 183:379–397, 1987.

[3] C. Basdevant, B. Legras, R. Sadourny, and M. Beland. A study of barotropic model flows: intermittency waves and predictability. *J. Atmos. Sci.*, 38:2305–2326, 1981.

[4] C. Basdevant and R. Sadourny. Modélisation des échelles virtuelles dans la simulation numérique des écoulements turbulents bidimensionels. *J. Méc. Théorique et Appl.*, Numéro spécial:243–269, 1983.

[5] G.K. Batchelor. Computation of the Energy Spectrum in Homogeneous Two-dimensional Turbulence. *Phys. Fluid, suppl. II*, 12:233–239, 1969.

[6] R. Benzi, G. Paladin, S. Patarnello, P. Santangelo, and A. Vulpiani. Intermittency and coherent structures in two–dimensional turbulence. *J. Phys. A: Math. Gen*, 19:3771–3784, 1986.

[7] R. Benzi, S. Patarnello, and P. Santangelo. Self–similarity of coherent structures in two–dimensional decaying turbulence. *J. Phys. A: Math. Gen*, 21:1221–1237, 1988.

[8] M. Cannone. *Ondelettes, Paraproduits et Navier–Stokes.* Diderot, 1995.

[9] Ph. Charton and V. Perrier. A Pseudo–Wavelet Scheme for the Two-Dimensional Navier–Stokes Equations. *Matematica Aplicada e Computacional*, 15, 1996.

[10] R.A. DeVore, B. Jawerth, and V. Popov. Compression of Wavelet Decomposition. *Americ. J. of Math.*, 114:737–785, 1992.

[11] M. Do-Khac, C. Basdevant, V. Perrier, and K. Dang-Tran. Wavelet analysis of 2D turbulent fields. *Physica D*, 76:252–277, 1994.

[12] F.W. Elliott and A.J. Majda. A new algorithm with plane waves and wavelets for random velocity fields with many spatial scales. *J. Comput. Phys.*, 117:146–162, 1995.

[13] M. Farge. Wavelet Transforms and their Applications to Turbulence. *Annu. Rev. of Fluid Mech*, 24:395–457, 1992.

[14] M. Farge, E. Goirand, Y. Meyer, F. Pascal, and M.V. Wickerhauser. Improved predictability of two-dimensional turbulent flows using wavelet packet compression. *Fluid Dynamics Research*, 10:229–250, 1992.

[15] M. Farge, Y. Guezennec, C.M. Ho, and C. Meneveau. Continuous wavelet analysis of coherent structures. In *Proceedings of the 1990 Summer Program*, pages 331–348. NASA-Ames and Stanford University, Center for Turbulence Research, 1990.

[16] M. Farge, N. Kevlahan, V. Perrier, and E. Goirand. Wavelets and Turbulence. *Proceedings of the IEEE, Special Issue on Wavelets*, 84, 1996.

[17] M. Farge and G. Rabreau. Transformé en ondelettes pour détecter et analyser les structures cohérentes das les écoulements turbulents bidimensionels. *C.R.Acad.Sci. Paris II*, 307:1479–1486, 1988.

[18] P. Federbush. Navier and Stokes meet the wavelet. *Comm. Math. Phys.*, 155:219–248, 1993.

[19] P. Frick and V. Zimin. Hierarchical Models of Turbulence. pages 265–283. Calderon Press, 1993.

[20] U. Frisch. *Turbulence. The legacy of A.N. Kolmogorov.* Cambridge University Press, 1995.

[21] J. Fröhlich and K. Schneider. An Adaptive Wavelet Galerkin Algorithm for One– and Two–Dimensional Flame Computations. *Eur. J. Mech., B/Fluids*, 13:439–471, 1994.

[22] J. Fröhlich and K. Schneider. A Fast Algorithm for Lacunary Wavelet Bases Related to the Solution of PDEs. *C. R. Math. Rep. Acad. Sci. Canada*, 16:83–86, 1995.

[23] J. Fröhlich and K. Schneider. An adaptive Wavelet–Vaguelette Algorithm for the Solution of Nonlinear PDEs. Technical Report SC 95-28, Konrad-Zuse-Zentrum für Informationstechnik Berlin, 1995. to appear in J. Comput. Phys.

[24] J. Fröhlich and K. Schneider. Numerical Simulation of Turbulent Flows in an Adaptive Wavelet Basis. Technical Report Dec. 95, Department of Chemistry University of Kaiserslautern, 1995. to appear in Appl. Comp. Harm. Anal.

[25] J. Jimenez, H.K. Moffatt, and C. Vasco. The structure of the vortices in freely decaying two–dimensional turbulence. *J. Fluid Mech.*, 313:209–222, 1996.

[26] N. Kevlahan. private communication, 1995.

[27] R.H. Kraichnan. Inertial Ranges in Two-dimensional Turbulence. *Phys. Fluids*, 10:1417–1423, 1967.

[28] M. Lesieur. *Turbulence in Fluids*. Kluwer Academic, 1990.

[29] J. Liandrat and F. Moret-Bailly. The wavelet transform. Some applications to fluid dynamics and turbulence. *Eur. J. Mech. B/Fluids*, 9:1–19, 1990.

[30] J. Liandrat and Ph. Tchamitchian. Resolution of the 1D regularized Burgers equation using a spatial wavelet approximation algorithm and numerical results. Technical report, ICASE, 1990.

[31] J.L. Lumley. The structure of inhomogeneous flows. In A.M. Yaglom and V.I. Tatarski, editors, *Atmospheric turbulence and radio wave propagation*. Moscow: Nauka, 1967.

[32] W.H. Matthaeus, W.T. Stribling, D. Martinez, S. Oughton, and D. Montgomery. Decaying, two-dimensional, Navier-Stokes turbulence at very long times. *Physica D*, 51:531–538, 1991.

[33] W.H. Matthaeus, W.T. Stribling, D. Martinez, S. Oughton, and D. Montgomery. Selective decay and coherent vortices in two–dimensional incompressible turbulence. *Phys. Rev. Lett.*, 66:2731–2734, 1991.

[34] C. Meneveau. Analysis of turbulence in the orthonormal wavelet representation. *J. Fluid Mech.*, 232:469–520, 1991.

[35] Y. Meyer. *Ondelettes et Opérateurs I/II*. Hermann, 1990.

[36] S.A. Orszag. Numerical Methods for the Simulation of Turbulence. *Phys. Fluids Suppl.II*, 12:250–257, 1969.

[37] S.A. Orszag. Numerical simulation of incompressible flows within simple boundaries I. Galerkin (spectral) representations. *Stud. Appl. Math.*, 50:293, 1971.

[38] V. Perrier and C. Basdevant. La décomposition en ondelettes périodiques, un outil pour l'analyse de champs inhomogènes. Théorie et algorithmes. *Rech. Aérosp.*, 1989-3:53–67, 1989.

[39] P. Santangelo, R. Benzi, and B. Legras. The generation of vortices in high resolution, two–dimensional decaying turbulence and the influence of initial conditions on the breaking of self–similarity. *Phys. Fluids*, 1:1027–1034, 1989.

[40] H. Tennekes and J.L. Lumley. *A first course in turbulence*. MIT Press, 1972.

[41] J.M. Vanel, R. Peyret, and P. Bontoux. A pseudo–spectral solution of vorticity–stream function equations using the influence matrix technique. In Morton and Baines, editors, *Numerical Methods for Fluid Dynamics*, pages 477–488. Clarendon Press, 1986.

[42] J.C. Mc Williams. The emergence of isolated coherent vortices in turbulent flows. *J. Fluid Mech.*, 146:21–43, 1984.

[43] J.C. Mc Williams. A demonstration of the suppression of turbulent cascades by coherent vortices in two–dimensional turbulence. *Phys. Fluids A*, 2:547–522, 1990.

[44] J.C. Mc Williams. The vortices of two–dimensional turbulence. *J. Fluid Mech.*, 219:361–385, 1990.

[45] V. Zimin. Hierarchical Model of Turbulence. *Izvestija, Atm. Ocean. Phys. (USA, translated from Russian)*, 17:941–949, 1981.